ACADEMIC PRESS

Available online at www.sciencedirect.com

SCIENCE DIRECT®

Journal of Sound and Vibration 269 (2004) 875–897

JOURNAL OF SOUND AND VIBRATION

www.elsevier.com/locate/jsvi

Study of airfoil gust response alleviation using an electro-magnetic dry friction damper. Part 2: Experiment

Deman Tang[a], Henri P. Gavin[b], Earl H. Dowell[a,*]

[a] *Department of Mechanical Engineering and Materials Science, Duke University, Box 90300, Durham, NC 27708-0300, USA*

[b] *Department of Civil and Environmental Engineering, Duke University, Box 90300, Durham, NC 27708-0300, USA*

Received 19 August 2002; accepted 9 January 2003

Abstract

In Part 1 of this work, a theoretical simulation study of the non-linear gust response of a three degree-of-freedom typical airfoil section with a control surface using an electro-magnetic dry friction damper is presented. For validation of this theoretical model, an electro-magnetic dry friction damper has been designed and an experimental investigation of the gust response has been carried out in a wind tunnel. Results for both periodic and linear frequency sweep gust excitations have been computed and measured. The fair to good quantitative agreement between theory and experiment verifies that the present electro-magnetic dry friction damper can be used to alleviate the gust response, especially for the plunge and pitch responses. It also shows that the present theoretical method can be successfully applied to determine the non-linear gust response when an electro-magnetic dry friction damper is used in the linear aeroelastic system.

© 2003 Elsevier Ltd. All rights reserved.

1. Introduction

In Part 1 of this work Ref. [1], a theoretical simulation study of the non-linear gust response of a three degree-of-freedom (d.o.f.) typical airfoil section with a control surface using an electro-magnetic dry friction damper is presented. To understand the fundamental physics of the non-linear aeroelastic response to a periodic or a linear frequency sweep gust excitation using this nonlinear damper, an experimental investigation is very important, not only to verify the theoretical results, but also to explore response characteristics not predicted by the available analytical methods.

*Corresponding author.
E-mail address: dowell@mail.ee.duke.edu (E.H. Dowell).

0022-460X/03/$ - see front matter © 2003 Elsevier Ltd. All rights reserved.
doi:10.1016/S0022-460X(03)00181-0

During the past several years, several types of semi-active electrorheological (ER) or magnetorheological (MR) dampers have been used for vibration attenuation of various dynamical systems. It has been shown that these dampers, when combined with appropriate control strategies, can be used to achieve improved performance of the dynamical system as described in the introduction of Part 1 [1].

The present MR damper design follows that of Ref. [2], although we did not use a magnetic flux with the fluid material to form the magnetic circuit. A simple damping device is constructed to generate a controllable dry friction force in an aeroelastic model. This damping device is called an electro-magnetic dry friction damper (EMD). The EMD device provides a non-linear dry friction damping force which can be represented by

$$f_D = f_d(I)\tanh\left(\frac{\dot{h}}{v_0}+\frac{h}{d_0}\right),$$

where $f_d(I)$ is an experimentally determined dry friction force amplitude which is dependent upon the current (I) of the EMD magnetic circuit and h and $\dot{h}$ are the input displacement and velocity variables.

A few years ago, a rotating slotted cylinder (RSC) gust generator was installed in the Duke University low-speed wind tunnel to generate a gust excitation field including either a sinusoidal gust or a linear frequency sweep gust excitation [3]. This apparatus provides an experimental tool to assess the accuracy of theoretical methods for determining response to gust loads.

A theoretical/experimental study of the aeroelastic response to a gust excitation for a three d.o.f. typical airfoil section with a freeplay in the control surface and non-linear stiffness in plunge or torsion directions has been made by the Duke team [4]. Here a first theoretical/experimental study of the non-linear aeroelastic response of a three d.o.f. typical airfoil with an electro-magnetic dry friction damper is conducted. In order to validate the theoretically predicted response characteristics of the non-linear aeroelastic system, an experimental investigation has been carried out in the Duke wind tunnel.

In Part 1 of the present paper a time-domain computer simulation method based upon a freeplay structural non-linearity in the control surface proposed in Ref. [4] is extended to calculate non-linear gust response with a damping non-linearity in the plunge direction when the time-correlated gust loads are known experimentally. Of course, the finite-state airloads model used considers the effect of gust loads on the aerodynamics as well as the motion-induced aerodynamics. Measured periodic and linear frequency sweep gust loads and experimental dynamic characteristics of an electro-magnetic dry friction damper are used in the theoretical calculations in this work.

The present experimental results are compared with those calculated from the companion paper, Part 1. The theoretical/experimental results may be helpful in better understanding physically the alleviation of a typical airfoil section response due to gust loads using an electro-magnetic dry friction damper.

2. Experimental model and controllable EMD

The experimental model consists of a two-dimensional NACA 0012 rectangular wing model mounted on support mechanisms including the EMD which are placed outside of the wind tunnel.

The wing model includes two parts: a main wing with a 19 cm chord and 52 cm span; and a control surface or flap with a 6.35 cm chord and 52 cm span, which is attached at the trailing edge of the main wing using two pairs of micro-bearings with a pin. A rotational axis composed of the micro-bearings and the pin allows the flap to have a rotational d.o.f. relative to the main wing. The pitch axis of the main wing is located at the quarter-chord. Both the torsional stiffnesses of the main wing and the flap can be adjusted.

The support mechanism at each end of the rectangular wing is a bi-cantilevered beam made of two steel leaf-springs which are 20.32 cm long, 2.86 cm wide, and 0.102 cm thick. The distance between the two cantilever beams is 15.24 cm. A support block joins the free ends of the bi-cantilever beams on both the top and bottom and is free to move in the plunge direction. Two EMDs are symmetrically mounted on both the top and bottom of the wind tunnel and the output end of each EMD is connected to the free end of the bi-cantilever beam through a steel plate and the magnetic powder. A schematic of the experimental model is shown in Part 1 [1, Fig. 1]. A gust generator is mounted in the wind tunnel. For the details of the generator, see Refs. [3,4]. A photograph of the experimental model with a gust generator is shown in Fig. 1.

The configuration of the EMD is shown in Fig. 2. The damping device consists of three parts: the first is an electro-magnetic generator caused by a spool wire in a low-carbon steel bar with two low-carbon steel blocks at the bar ends. This generator can be rigidly fixed (without a force measurement system) or elastically fixed (with a force measurement system). The second is a low-carbon steel plate which is fixed to the plunge spring system of the aeroelastic model. There is a gap between the steel blocks of the electro-magnetic generator and the steel plate. The third is the special magnetic material powder (carbonyl iron powder) which fills the gap. The carbonyl iron powder (BASF #819011, Mount Olive, NJ) is mono-disperse with a mean diameter of about 5 μm. In this system, a controllable dry friction force can be obtained that depends on the dimensions of the damping device and the input current.

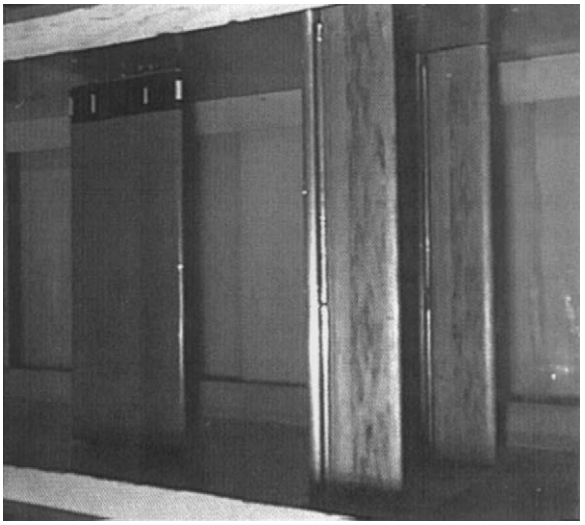

Fig. 1. Experimental aeroelastic model with EMD and gust generator in the wind tunnel.

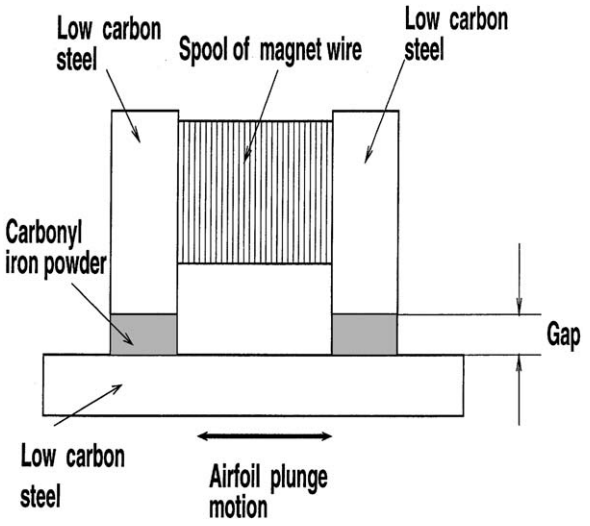

Fig. 2. Configuration of the EMD.

3. Experimental study of the EMD damping device

Fig. 2 illustrates the conceptual design of the EMD. The bar, block and plate are made of low-carbon steel. The bar length is 4.2 cm and the diameter is 2.54 cm. The block dimensions are $1.5 \times 2.54 \times 3.2$ cm^3. The surface area of the magnetic powder is 1.5×2.54 cm^2. The 24-gage magnet wire is spooled on a bar. The number of turns is 300 over the bar length. The two blocks are attached to the ends of the bar by a bolt. The plate dimensions are $3.8 \times 8.9 \times 0.32$ cm^3. Two gap values between the block and plate are selected as 0.5 mm and 1.5 mm. For the measurement of the damping force, the magnetic spool is elastically fixed by the bi-cantilever beams. The natural frequency of the magnetic spool is 75 Hz. Two strain gages are glued to the root of the bi-cantilever beams to measure the damping force.

For the dynamic test of the EMD damping device, the steel plate is fixed on a shake table. The vibration amplitude of the shake table is 0.28 or 0.14 cm for a gap = 0.5 mm or 0.25 cm for a gap = 1.5 mm. The excitation frequency can be adjusted by LabView 5.1 software and a computer. The experimental setup is shown in Fig. 3.

3.1. *Results for gap = 0.5 mm*

Fig. 4(a) shows a measured time history (broken line) of the damping force for an input current of 1.0 A and an excitation frequency of 2 Hz with an excitation amplitude of 0.28 cm. The damping force shows dry friction behavior. The transient force responses due to the free oscillation of the damping device also appear in the force output signal. In order to eliminate the transient force responses (when the magnetic spool is rigidly fixed), a low pass filter is added to the measurement system. We used two 4302 Dual 24 db/Octave filters in the test. The cutoff frequency is 40 Hz and the gain is 1. The phase shift error due to the low pass filter itself is eliminated because we filter both the input and output signals. The result is shown by a dashed–dot line in

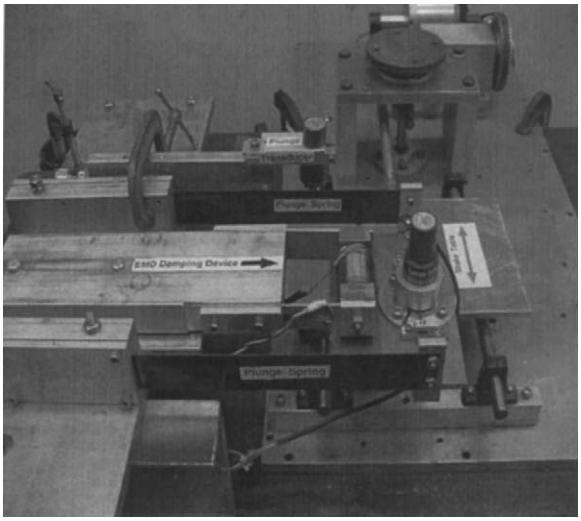

Fig. 3. Photograph of the experimental setup of the EMD damping device.

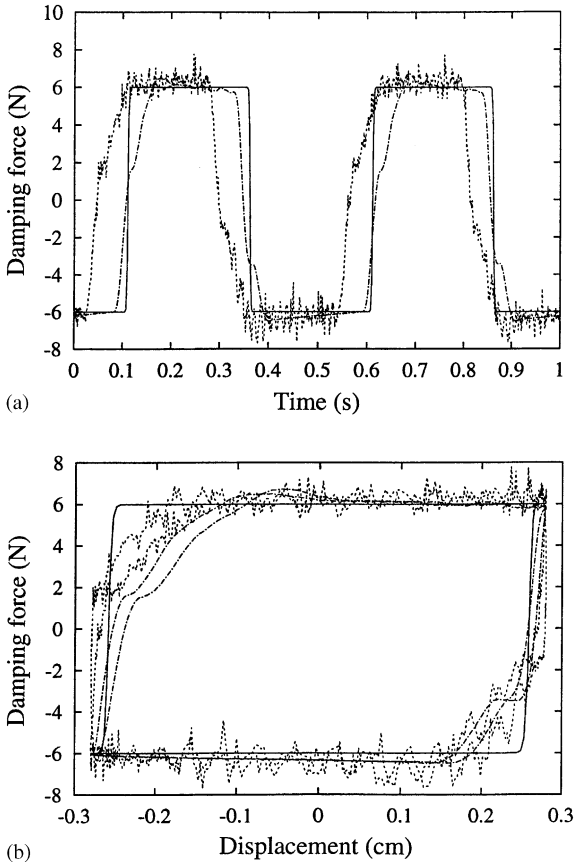

Fig. 4. Damping force behavior at an excitation frequency of 2 Hz, amplitude of 0.28 cm and input current of 1 A: (a) for time history and (b) for damping force vs. displacement;—, theory; ⋯, test; – · –, test filtered.

Fig. 4(a). To compare to the filtered measurement data, a numerical simulation is made using Part 1 [1, Eq. (14)].

In order to obtain the optimized parameters, v_0 and d_0, for the damper model from the above experimental data, a least-squares optimization method is used. The parameters are estimated by minimizing the error between the model-predicted force and the force from the experimental data. The parameters are chosen as $v_0 = 0.13$ cm/s and $d_0 = 0.024$ cm. The theoretical result is shown by a solid line and the theoretical damping force is close to the filtered measurement force.

Fig. 4(b) shows the damping force vs. displacement for the same case. The hysteresis behavior is evident.

When the excitation frequency increases to 4 Hz and the excitation amplitude decreases to 0.14 cm (note that the velocity amplitudes are the same for the two cases), the results are shown in Fig. 5 for an input current of 1 A. It is found that the two results (Figs. 4 and 5) are very similar and have the same damping force values. The selected theoretical parameters in Fig. 4 are also the

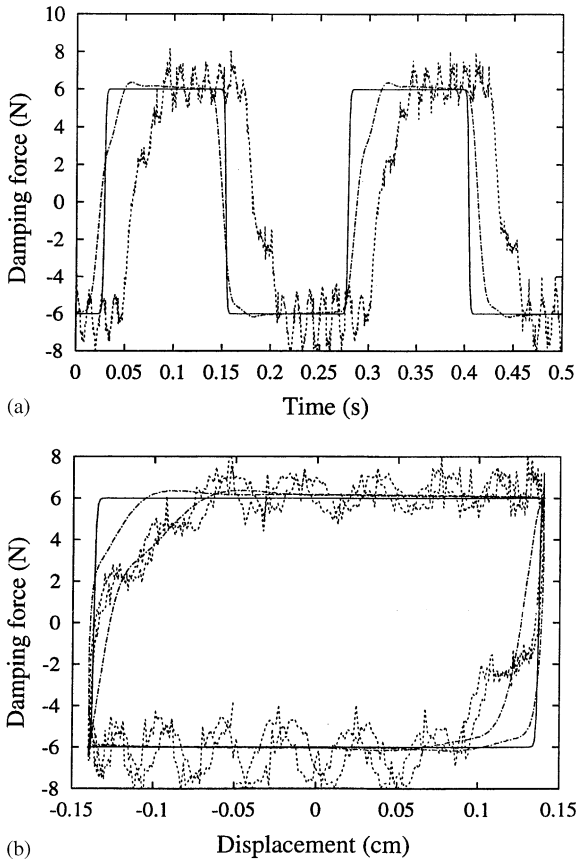

Fig. 5. Damping force behavior at an excitation frequency of 4 Hz, amplitude of 0.14 cm and input current of 1 A: (a) for time history and (b) for damping force vs. displacement; —, theory; ⋯, test; – · –, test filtered.

same as those used for Fig. 5. The damping force is almost independent of the excitation condition when the input current is constant.

Fig. 6(a) shows the measured time history (after filtering) of the damping force vs. various input currents, 0.5, 1.0 and 1.5 A, for an excitation frequency of 2 Hz and an amplitude of 0.28 cm. Correspondingly, the damping force vs. displacement is shown in Fig. 6(b). It is found that the damping force amplitude increases as the input current increases, but the hysteretic behavior of the damping force does not change significantly. Similar results are shown in Fig. 7 for an excitation frequency of 4 Hz and an amplitude of 0.14 cm.

Fig. 8 shows the measured damping force amplitude vs. the excitation velocity amplitude from 2 to 14 m/s for input currents from 0 to 1.5 A. The excitation amplitude is fixed at 0.28 cm; the excitation frequency is variable. The damping force is almost independent of the velocity amplitude for a given input current. This experimentally determined damping force can be provided by the present EMD damping device to the airfoil aeroelastic system.

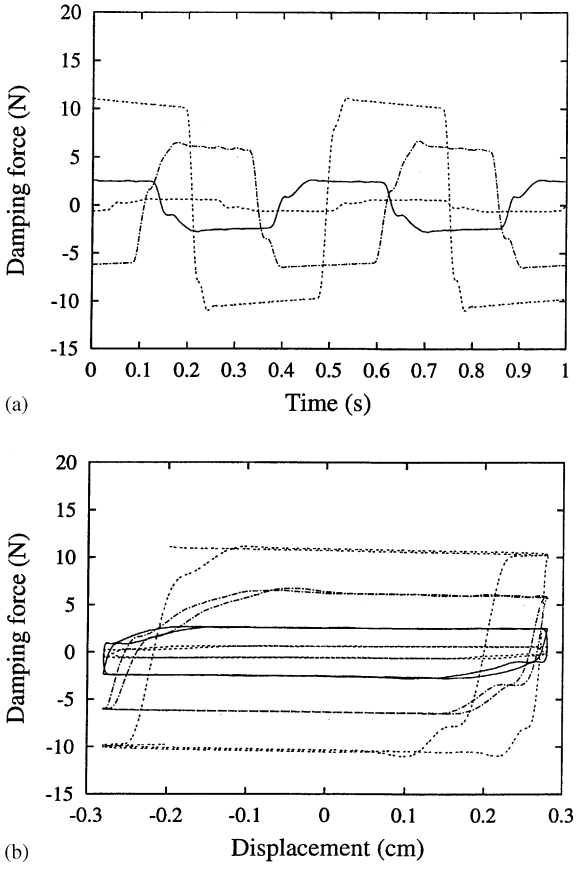

Fig. 6. Damping force behavior at an excitation frequency of 2 Hz and an amplitude of 0.28 cm for several input currents: (a) for time history and (b) for damping force vs. displacement; ⋯, 0.0 A; —, 0.5 A; – · –, 1.0 A; - -, 1.5 A.

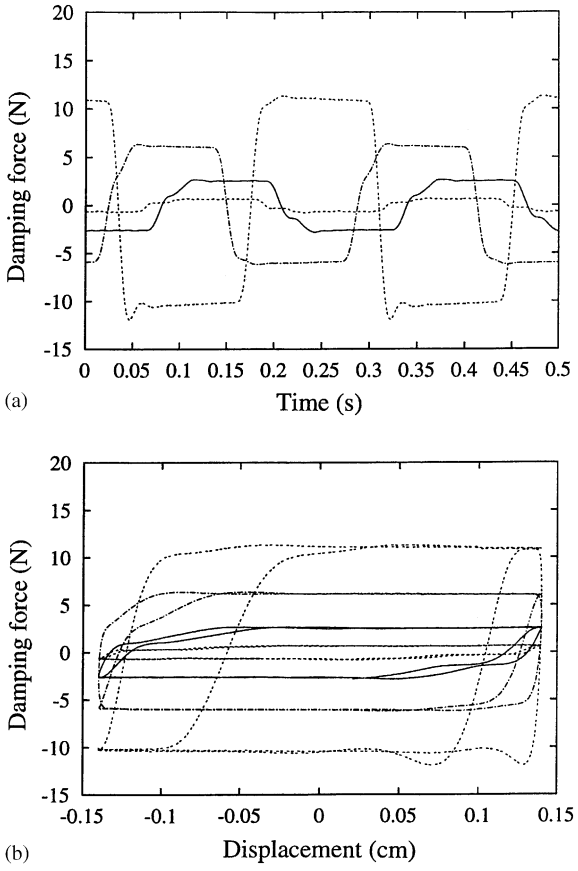

Fig. 7. Damping force behavior at an excitation frequency of 4 Hz and an amplitude of 0.14 cm for several input currents: (a) for time history and (b) for damping force vs. displacement; ⋯, 0.0 A; —, 0.5 A; – · –, 1.0 A; - -, 1.5 A.

3.2. *Results for gap* = 1.5 *mm*

Fig. 9(a) shows a measured (after filtering) time history (broken line) of the damping force for an input current of 1.0 A and an excitation frequency of 5 Hz with an excitation amplitude of 0.25 cm.

Also, a least-squares optimization method is used to determine the damper model parameters. The parameters are chosen as $v_0 = 2.2$ cm/s and $d_0 = 0.08$ cm. The theoretical and experimental damping forces vs. the displacement are shown in Fig. 9(b). The theoretical damping force is close to the measured force.

Fig. 10(a) shows the measured time history (after filtering) of the damping force vs. various input currents, 0, 0.5, 1.0 and 1.5 A, for an excitation frequency of 5 Hz and an amplitude of 0.25 cm. Correspondingly, the damping force vs. displacement is shown in Fig. 10(b). The damping force behavior is similar to that of Figs. 6 and 7 for a gap = 0.5 mm, but the damping force level decreases as the gap increases.

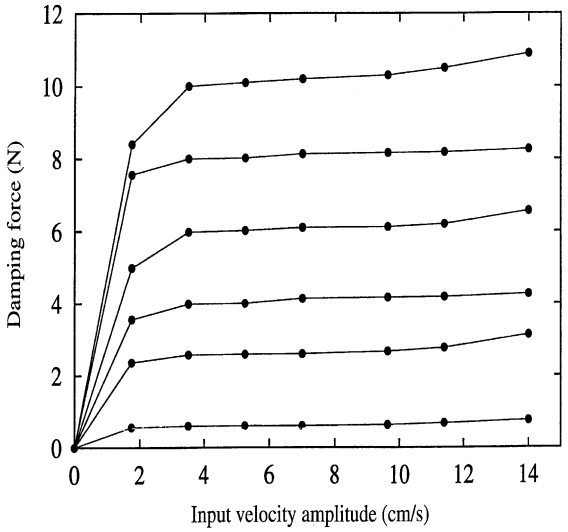

Fig. 8. Damping force amplitude vs. input velocity for several input currents: 0.0, 0.5, 0.75, 1.0, 1.25 and 1.5 A (from bottom to top).

Fig. 11 shows the measured damping force amplitude vs. the excitation velocity amplitude from 2 to 14 m/s for input currents from 0 to 1.5 A. The excitation amplitude is fixed at 0.25 cm; the excitation frequency is variable. The damping force is almost independent of the velocity amplitude for a given input current.

Fig. 12 shows the measured damping force amplitude vs. the input current from 0 to 2 A for an excitation frequency of 2 Hz, an amplitude 0.28 cm, and a gap = 0.5 mm or an excitation frequency of 5 Hz, an amplitude 0.25 cm, and a gap = 1.5 mm, respectively. The damping force amplitude increases with increasing input current. However, in the larger current range (larger than 1.5 A), the damping force increases more slowly for the small gap case. This is because in this range the system becomes magnetically saturated.

4. Theoretical and experimental correlation for the aeroelastic model

The parameters of the theoretical model come from the experimental model previously described in Part 1 [1]. The nominal values for the inertial, stiffness, and damping parameters of the experimental structural system were measured. A summary of the system parameters is given in Part 1 [1, Table 1]. A comparison of the theoretical and experimental structural natural frequencies (without the EMD damping device) is given in Table 1.

In this paper we discuss the theoretical and experimental correlations for the non-linear responses to both periodic and linear sweep frequency gust excitations and the gust response alleviation by using an electro-magnetic dry friction damper. In order to obtain a more meaningful correlation between theory and experiment, the gust angle of attack for the periodic and frequency sweep gust excitations is measured and quantitatively calibrated.

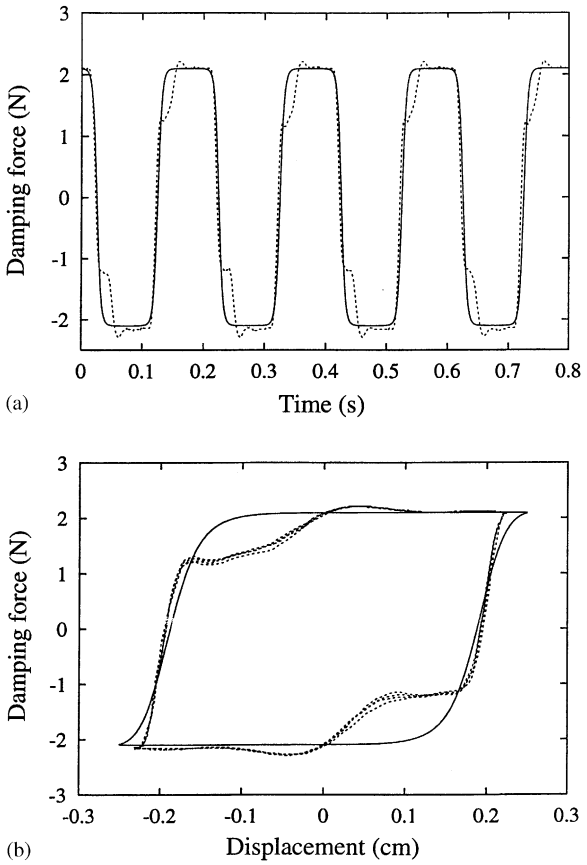

Fig. 9. Theoretical and experimental damping force behavior at an excitation frequency of 5 Hz and an amplitude of 0.25 cm for a gap = 1.5 mm and $I = 1$ A: (a) for time history and (b) for damping force vs. displacement; —, theory; ⋯, test.

4.1. Correlation for a periodic gust excitation

Fig. 13 shows a typical measured gust strength (α_g) vs. gust excitation frequency (Hz) for the flow velocity $U = 20$ m/s. In this figure, the symbol ◦ indicates the measured first harmonic component and the symbol • indicates the second harmonic component. The solid line indicated the least-squares curve fitting from the experimental data. The gust strength varies with the gust frequency and is not a pure sinusoid. The second harmonic component should not be neglected. In the theoretical calculations we use the measured experimental gust load for comparison with the experimental results.

First, consider the correlation between theoretical and experimental results without the EMD. The theoretical and experimental results for the plunge, pitch and flap responses are shown in Figs. 14(a), (b) and (c) for the flow velocity $U = 20$ m/s. The excitation frequency is controlled by the DC-motor. For each frequency excitation, the total sampling length is 1024 points after the steady response is achieved. The r.m.s. value is calculated from the total sampling points.

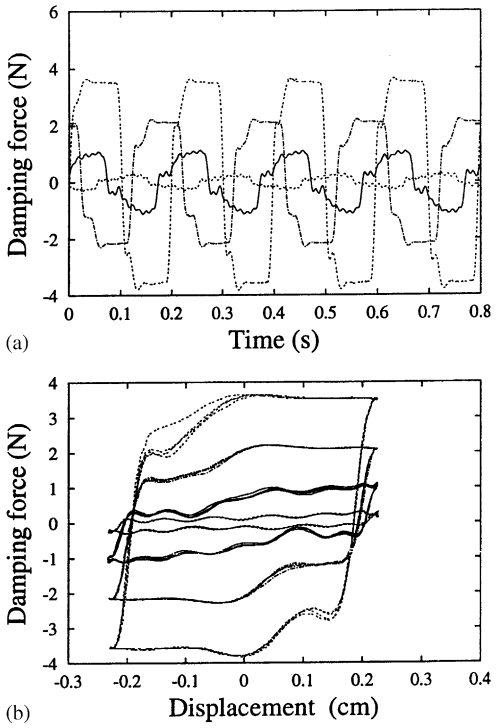

Fig. 10. Damping force behavior at an excitation frequency of 5 Hz and an amplitude of 0.25 cm for gap = 1.5 mm and several input currents: (a) for time history and (b) for damping force vs. displacement; ⋯, 0.0 A; —, 0.5 A; – · – 1.0 A; – –, 1.5 A.

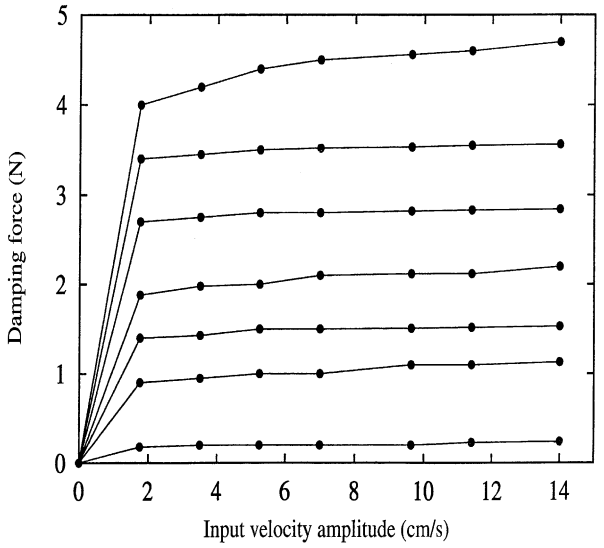

Fig. 11. Damping force amplitude vs. input velocity for several input currents: 0.0, 0.5, 0.75, 1.0, 1.25 and 1.5 A (from bottom to top).

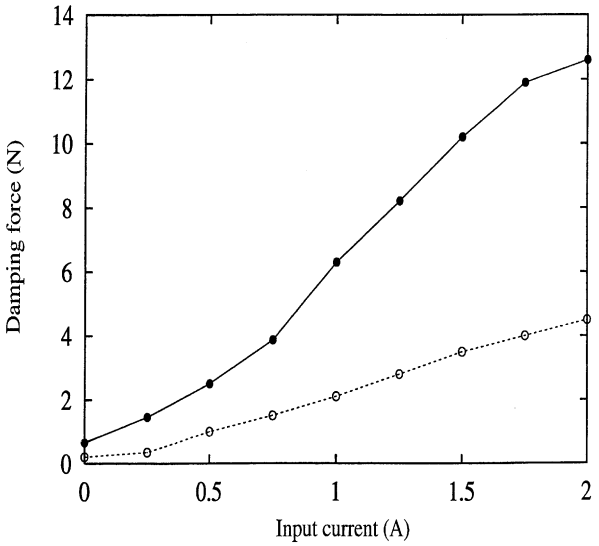

Fig. 12. Damping force amplitude vs. input current: –●–, gap = 0.5 (mm); · · ◦ · ·, gap = 1.5 (mm).

Table 1
Frequencies

	Computed (Hz)	Experimental (Hz)	% Difference
ω_α (coupled)	7.91	8.1	2.4
ω_β (coupled)	17.08	17.2	0.7
ω_h (coupled)	4.07	4.12	1.2

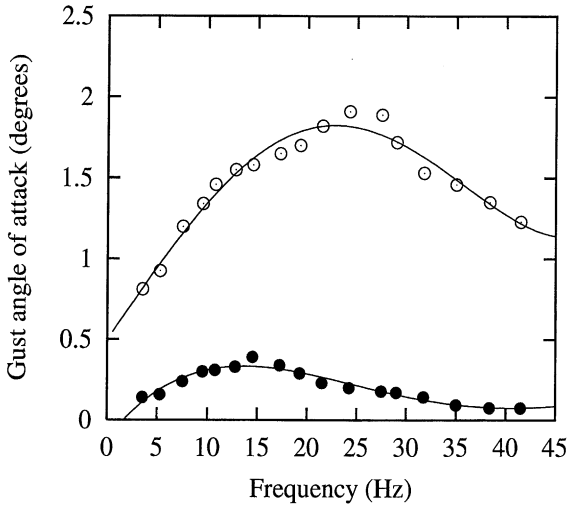

Fig. 13. A periodic gust excitation for $U = 20$ m/s: ◦ and —, 1st harmonic; ● and —, 2nd harmonic.

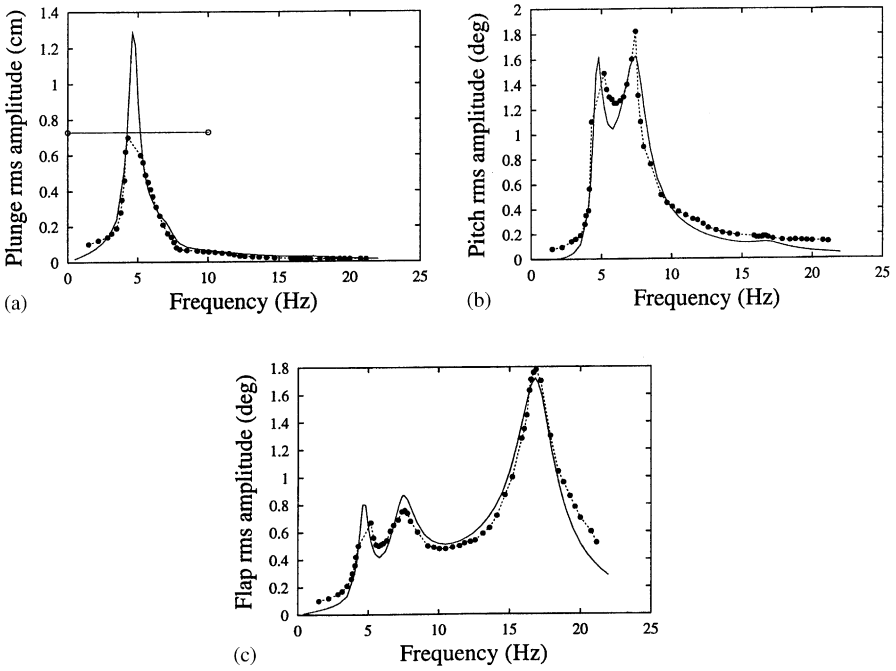

Fig. 14. Theoretical and experimental frequency responses to a periodic gust for a model without EMD and a flow velocity of 20 m/s: (a) for plunge, (b) for pitch and (c) for flap; —, theory; · · ● · ·, test; ○—○, plunge limiting boundary.

The plunge response has a very large amplitude near the plunge resonant frequency (4.8 Hz). A device to limit motion is mounted to protect this aeroelastic model. The limiting motion boundary in plunge is set to be ± 1.1 cm.

In these figures, both theoretical (solid line) and experimental (●, plus dashed line) results are shown for the correlation between theory and experiment. It is very clear that the plunge, pitch and flap resonant frequencies are 4.8, 7.4 and 16.5 Hz for this aeroelastic system. The theoretical and experimental results are reasonably close. It should be noted that there is a small peak at the half plunge resonant frequency (2.4 Hz). This is because of the second harmonic gust excitation.

Figs. 15(a)–(c) show the theoretical and experimental frequency responses for the aeroelastic model with an EMD vs. the several damping force levels $f_d = 1, 2$ N and the flow velocity is 20 m/s. Also the results without the EMD are shown in these figures. When $f_d = 1$ N, the plunge amplitude evidently decreases near the plunge resonant frequency. The maximum plunge peak moves to about 5 Hz. The pitch peak response at the plunge resonant frequency disappears. However, the peak response near the pitch resonant frequency increases compared to the case for no EMD. When $f_d = 2$ N, the plunge amplitude significantly decreases. The plunge resonant frequency moves to 7 Hz, near the pitch resonant frequency, while the pitch response reaches a maximum value. Also the pitch response near the resonant frequency increases compared to the cases for no EMD and also for an EMD with $f_d = 1$ N. The flap responses near the flap resonant frequency have a slight increase when the damping force level increases. The agreement between the theoretical and experimental results is reasonably good.

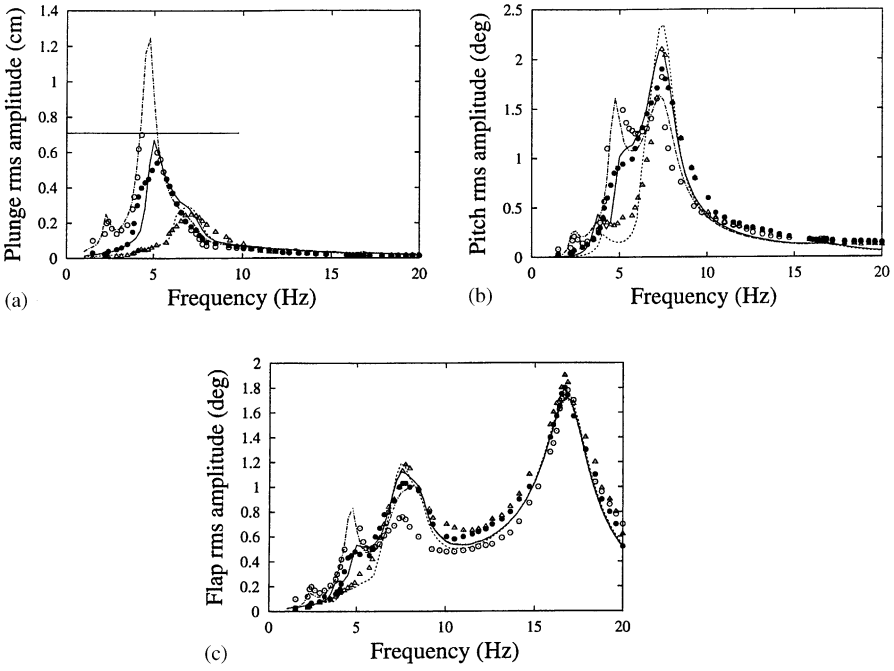

Fig. 15. Theoretical and experimental correlation for $f_d = 1, 2$ N and a flow velocity of 20 m/s: (a) for plunge, (b) for pitch and (c) for flap. Theory: ---, $f_d = 0$; —, $f_d = 1$ N; ⋯, $f_d = 2$ N. Test: ◦, $f_d = 0$; •, $f_d = 1$ N; △, $f_d = 2$ N; —-, plunge limiting boundary.

Figs. 16(a)–(c) show the experimental time history for plunge, pitch and flap responses at a gust excitation frequency of 5.18 Hz and several dry friction damping levels, $f_d = 0, 1$ and 2 N. Figs. 16(d) and (e) show the corresponding time history for the damping force with $f_d = 1$ and 2 N and the hysteresis loop of the damping force. At this gust frequency, the responses decrease as the damping force level increases. When $f_d = 2$ N, the damping force has a local "stick" behavior as shown in Fig. 16(d). In this condition, the hysteresis loop of the damping force provides less energy dissipation per 1 cycle of the plunge motion, but it provides a larger additional plunge stiffness and thus changes the system dynamic behavior. The plunge response becomes smaller.

Figs. 17(a)–(c) show the experimental time history for plunge, pitch and flap responses at a gust excitation frequency of 7.4 Hz and several dry friction damping levels, $f_d = 0$, 1 and 2 N. Figs. 17(d) and (e) show the corresponding time history for the damping force with $f_d = 1$ and 2 N and the hysteresis loop of the damping force. At this gust frequency (very near the pitch resonant frequency), the responses increase as the damping force level increases. Due to the action of the larger aerodynamic forces (note that the aerodynamic forces are more sensitive to the pitch angle change than the plunge change), all system responses increase although the hysteresis loop of the damping force provides more energy dissipation than the "stick" condition. But the increase of the pitch response is smaller due to the balance between the energy dissipation and system dynamics change.

Figs. 18(a)–(c) show the experimental time history for plunge, pitch and flap responses at a gust excitation frequency of 16.5 Hz and several dry friction damping levels, $f_d = 0, 1$ and 2 N. At this

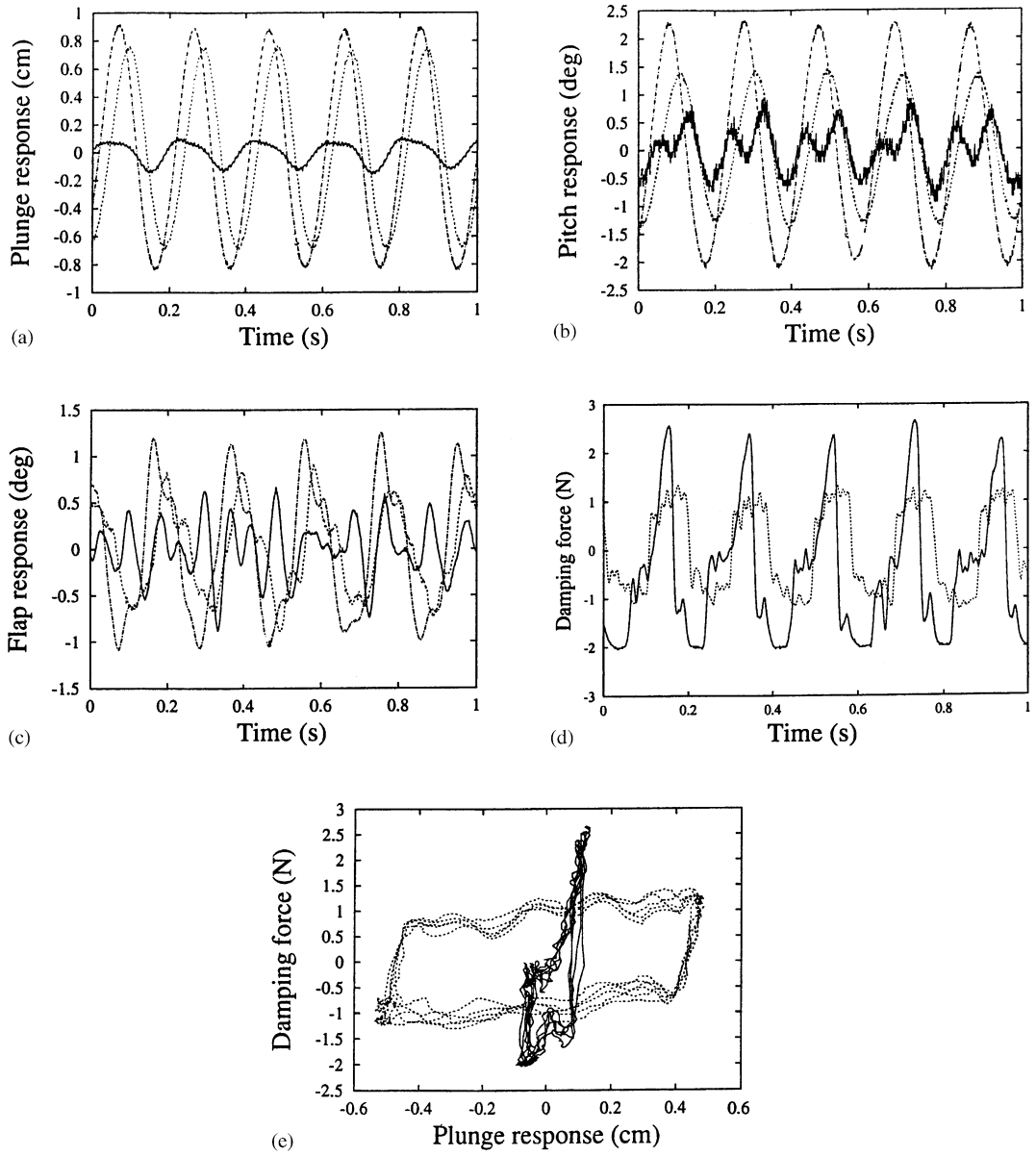

Fig. 16. Experimental results at a gust frequency of 5.18 Hz and a flow velocity of 20 m/s for several non-linear damping levels: (a) plunge response, (b) pitch response, (c) flap response, (d) damping force and (e) hysteresis loop; ---, $f_d = 0$; ⋯, $f_d = 1$ N; —, $f_d = 2$ N.

gust frequency (very near the flap resonant frequency), the plunge and pitch responses decrease as the damping force level increases and the responses are smaller especially for the plunge motion. The damping device is almost in a "stuck" condition and no hysteresis damping contributes to the

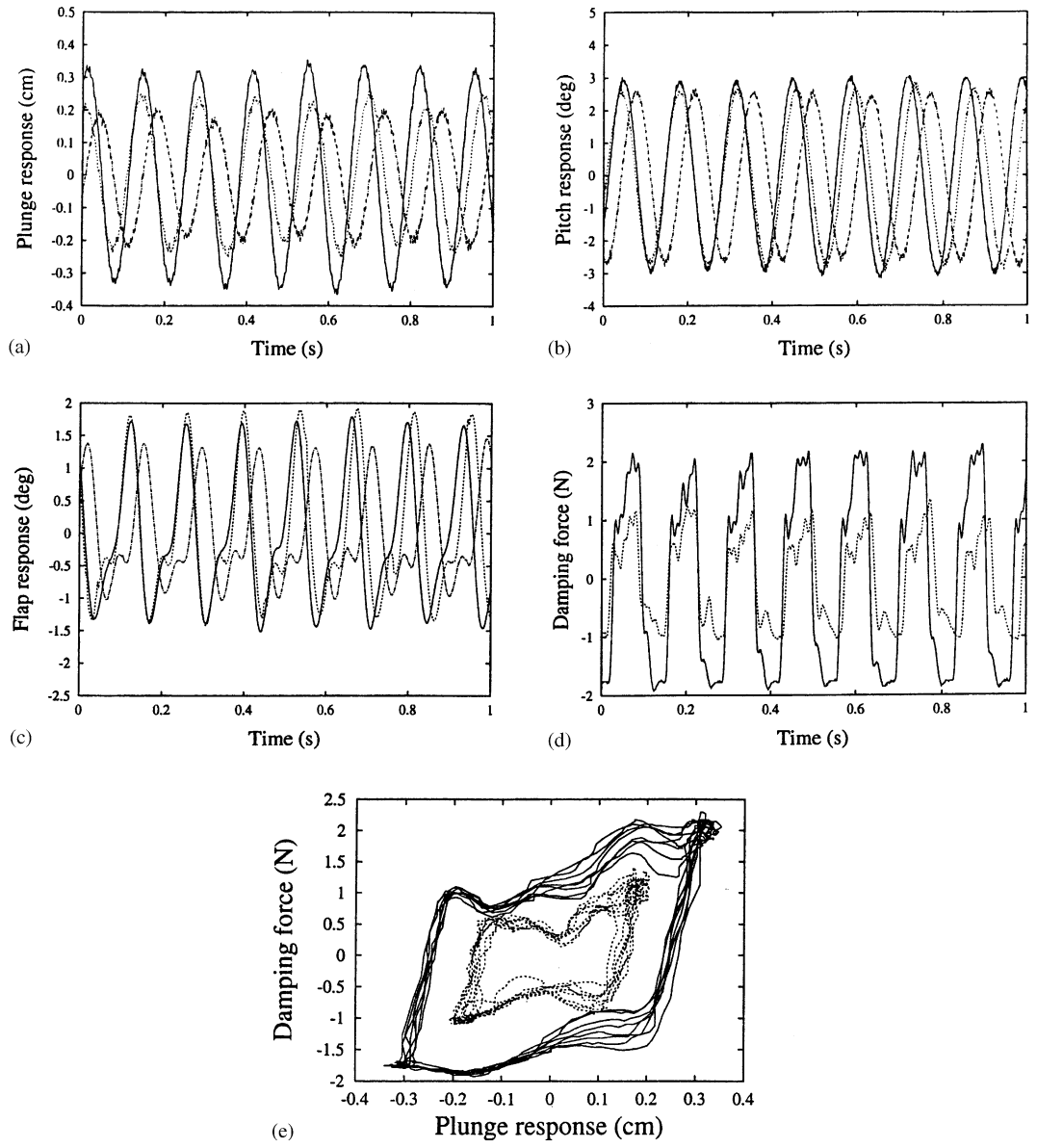

Fig. 17. Experimental results at a gust frequency of 7.4 Hz and a flow velocity of 20 m/s for several non-linear damping levels: (a) plunge response, (b) pitch response, (c) flap response, (d) damping force and (e) hysteresis loop; ---, $f_d = 0$; ⋯, $f_d = 1$ N; —, $f_d = 2$ N.

dynamic system. However, the flap rotation response has a smaller increase due to the system change caused by the additional stiffness "constraint" created by the damping device.

From the above theoretical and experimental observation and analysis, it is found that the damping device provides different contributions to the dynamic system for different gust excitation frequencies. One can use an alleviation ratio, η_f, defined in Part 1 [1] of the companion

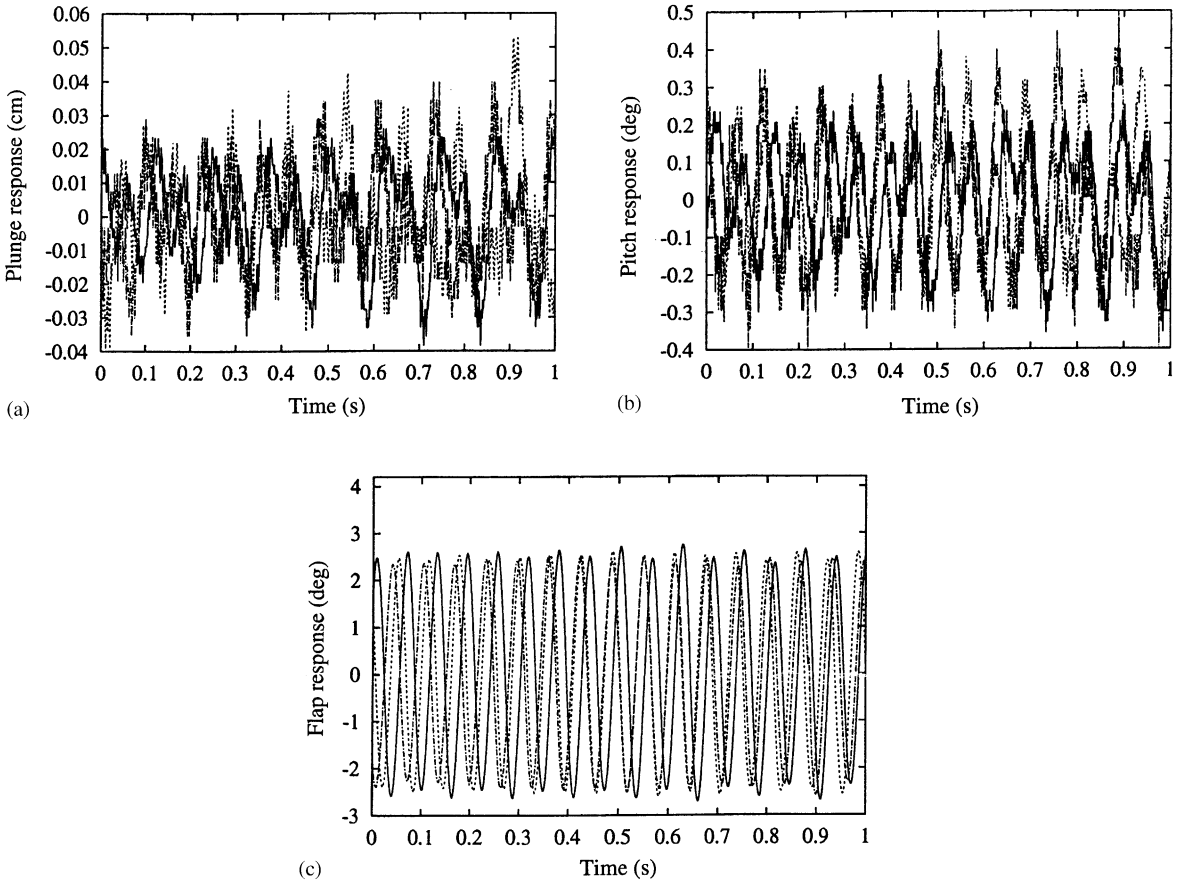

Fig. 18. Experimental results at a gust frequency of 16.5 Hz and a flow velocity of 20 m/s for several non-linear damping levels: (a) plunge response, (b) pitch response, (c) flap response; ---, $f_d = 0$; ⋯, $f_d = 1$ N; —, $f_d = 2$ N.

paper to calculate an averaged frequency response to a periodic gust. The theoretical and experimental results are shown in Fig. 19, where the total sample frequency number, m, is 100 for the theory and 55 for the test and $\omega_0 = 1$ Hz, $\omega_m = 20$ Hz. The plunge response alleviation is very evident. The pitch response alleviation is moderate. Although there is local maxima at some gust frequencies, the average frequency response over the total gust frequency band still decreases as the damping force level increases. The flap response alleviation is slight. The agreement between the theoretical and experimental results is reasonably good.

4.2. Correlation for a frequency sweep gust excitation

Fig. 20(a) shows a measured continuous linear frequency sweep gust angle of attack for $U =$ 20 m/s. The gust strength (angle of attack) is variable with time as expected from theory. For the measured lateral gust, the minimum and maximum frequencies are 0 and 40 Hz, and the sweep duration T is 3 s. For convenient application in the gust response analysis, a formula based on the

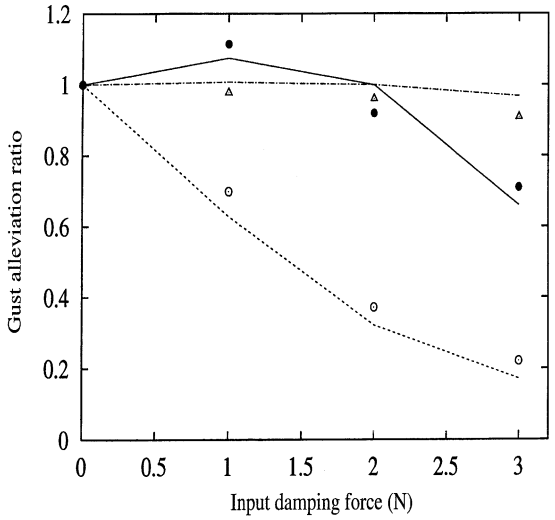

Fig. 19. Alleviation ratio, η_f, for the frequency response to a periodic gust. Theory: ⋯, plunge; —, pitch; -·-, flap. Test: ◦, plunge; •, pitch; △, flap.

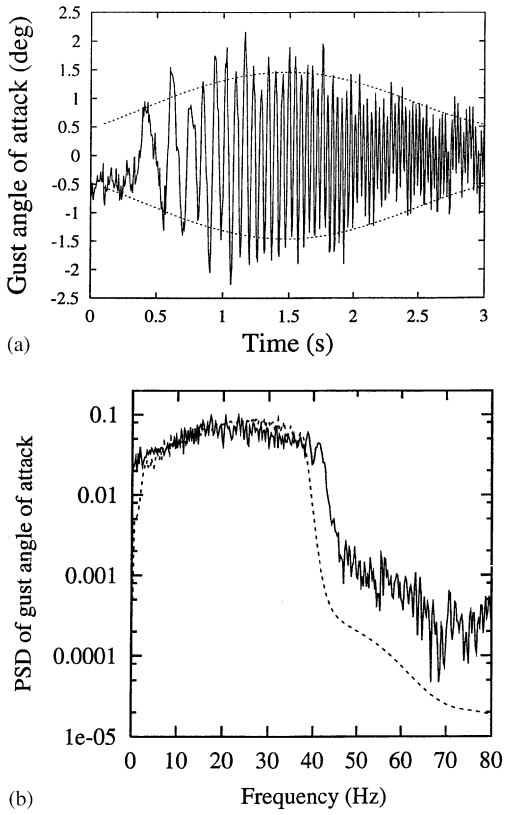

Fig. 20. Frequency sweep gust excitation for $U = 20$ m/s: (a) for time history and (b) for PSD; —, test; ⋯, simulation.

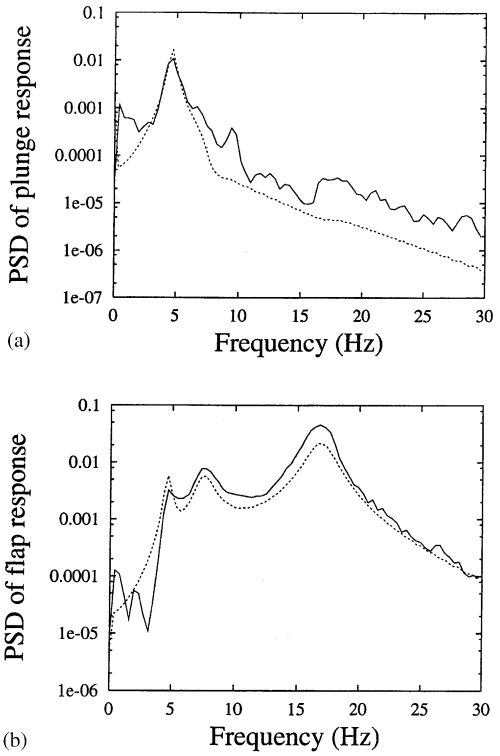

Fig. 21. Theoretical and experimental PSD response to a sweep frequency gust for a model without EMD at a flow velocity of 20 m/s: (a) plunge and (b) flap response; —, test; ⋯, theory.

experimental gust angle of attack data is constructed,

$$\alpha_g(t) = \bar{\alpha}_g(t) \sin\left(\omega_1 + \frac{\omega_2 - \omega_1}{2T} t\right) t, \tag{1}$$

where $\alpha_g(t)$ is given by

$$\bar{\alpha}_g(t) = \sum_{i=0}^{4} c_i t^i, \tag{2}$$

and $c_0, \ldots, c_4$ are determined by the least-squares curve fitting method applied to the experimental data.

An envelope of the numerical gust simulation is plotted in Fig. 20(a) as indicated by the broken line.

Fig. 20(b) shows a corresponding power spectra density (PSD) plot and a comparison between the measured continuous linear frequency sweep gust (solid line) and the numerical gust simulation (broken line) for $U = 20$ m/s. The experimental PSD is based on an average over 10 sweep periods. The power spectra density is almost constant in the frequency range of 40 Hz. Thus, this gust spectra can be used to simulate a white noise within a certain frequency band range.

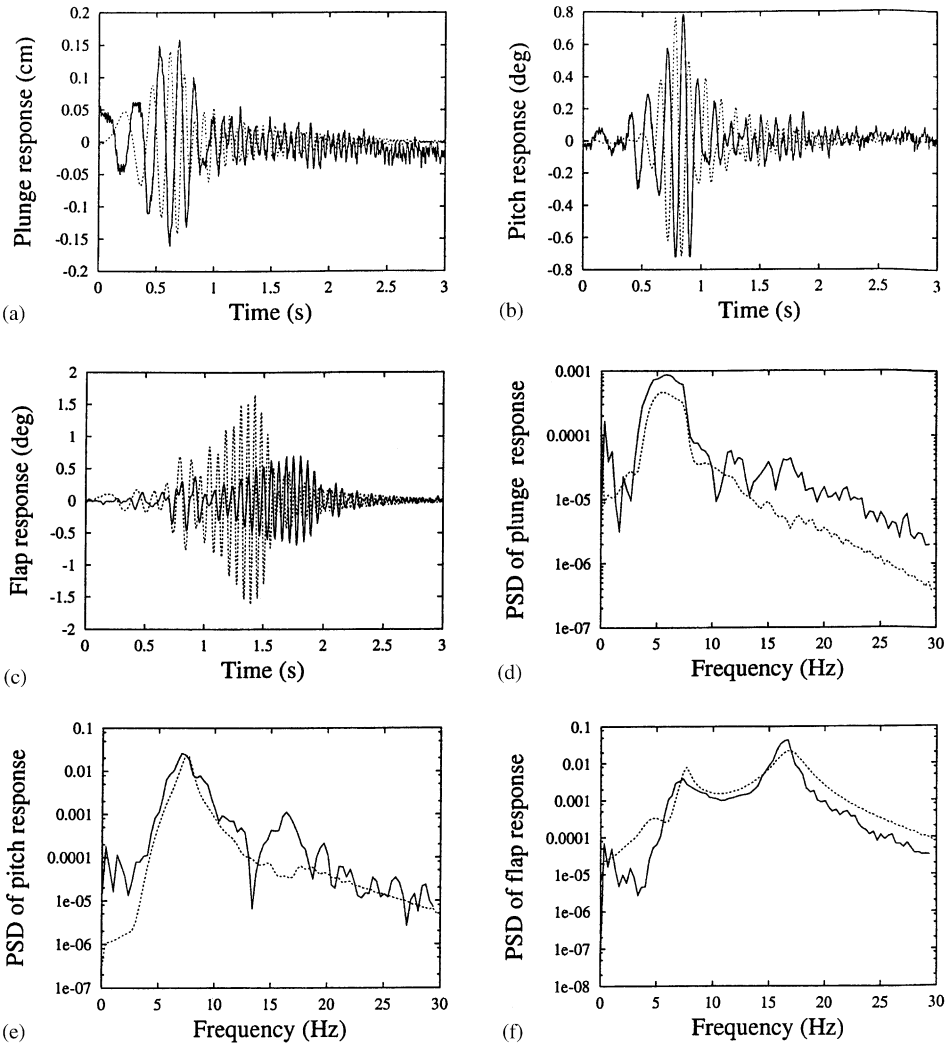

Fig. 22. Theoretical and experimental correlation for $f_d = 1$ N and a flow velocity of 20 m/s: (a) plunge response, (b) pitch response, (c) flap response, (d) plunge PSD, (e) pitch PSD and (f) flap PSD; —, test; ···, theory.

Eqs. (1) and (2) are used as theoretical gust excitations to calculate the non-linear gust response for comparison with the experimental response results.

First, consider the correlation between theoretical and experimental results without the EMD. The theoretical and experimental PSD results for the plunge and flap responses are shown in Figs. 21(a) and (b) for the flow velocity $U = 20$ m/s. There are 10 sweep periods in 32 s and the total sampling length is 5472 points for the experimental data. Note that the measured lateral gust has about a 0.2 s time delay corresponding to the restarting time of the DC-motor for each repeated sweep due to its rotational inertia. The actual useful total sampling length is 5120 points and 512 points per sweep frequency cycle.

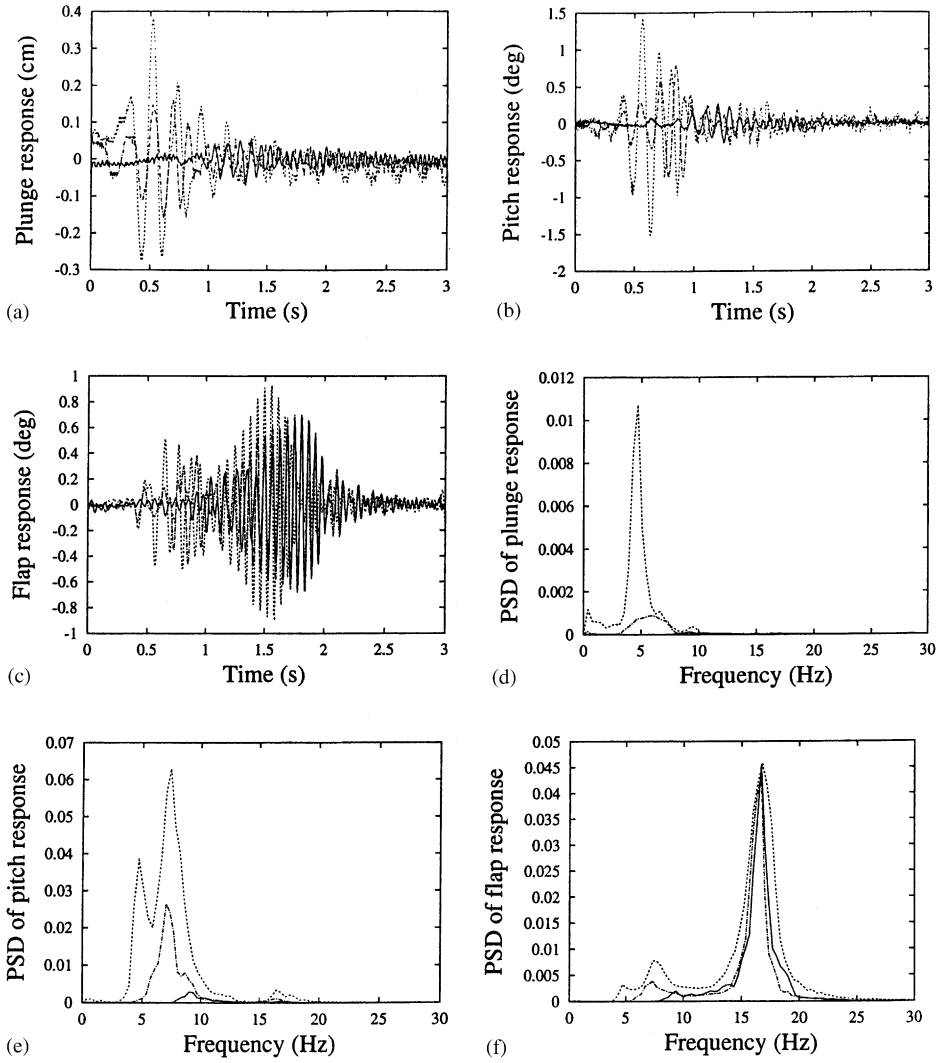

Fig. 23. Experimental results for a flow velocity of 20 m/s and several non-linear damping levels: (a) plunge response, (b) pitch response, (c) flap response, (d) plunge PSD, (e) pitch PSD and (f) flap PSD; ⋯, $f_d = 0$; ---, $f_d = 1$ N; —, $f_d = 2$ N.

In this figure, both theoretical (dashed line) and experimental (solid line) results are shown for an average over 10 sweep periods. It is very clear that the plunge, pitch and flap resonant frequencies are 4.8, 7.4 and 16.5 Hz for this aeroelastic system. The theoretical and experimental results are reasonably close.

Fig. 22 shows the typical theoretical and experimental results for the aeroelastic model with an EMD at $f_d = 1$ N and a flow velocity of 20 m/s. Figs. 22(a)–(c) show the time history for plunge, pitch and flap responses and the corresponding averaged PSD analysis are shown in Figs. 22(d)–(f). Note that only one sweep period is shown for the time response. The agreement between the theoretical and experimental results is reasonably good.

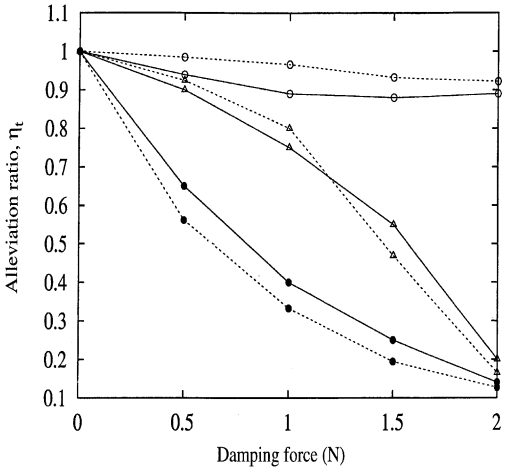

Fig. 24. Alleviation ratio, η_t, for the time response to a sweep frequency gust. Test: –○–, flap; –△–, pitch; –●–, plunge. Theory: · · ○ · ·, flap; · · △ · ·, pitch; · · ● · ·, plunge.

Fig. 23 shows the experimental results for a flow velocity of 20 m/s and several dry friction damping levels, $f_d = 0, 1$ and 2 N. Figs. 23(a)–(c) show the time history for plunge, pitch and flap responses and the corresponding averaged PSD are shown in Figs. 23(d)–(f). Note that the PSD co-ordinate used here is a linear co-ordinate rather than a logarithm. It is found that the plunge and pitch responses to a sweep gust load decreases as the non-linear damping force increases. However, the flap rotation response does not. The electro-magnetic dry friction damper mounted in the plunge direction can significantly alleviate the plunge and pitch responses under a sweep frequency gust.

One can define an alleviation ratio, η_t, described in Part 1, Ref. [1], for the time response to a sweep frequency gust. The theoretical and experimental results are shown in Fig. 24, where a total sample number (time series number), m_t, is taken as 5120. The plunge and pitch response alleviations are very evident. The flap response alleviation is slight. The agreement between the theoretical and experimental results is reasonably good.

5. Conclusions

An electro-magnetic dry friction damper has been designed and tested. The non-linear gust response of a three d.o.f. typical airfoil section with a control surface using this non-linear damper has been studied theoretically and experimentally. Results for both periodic and linear frequency sweep gust excitations have been computed and measured. The fair to good quantitative agreement between theory and experiment verifies that the present electro-magnetic dry friction damper can be used to alleviate the gust response, especially for the plunge and pitch responses. It also shows that the present theoretical method can be successfully applied to determine the non-linear gust response when an electro-magnetic dry friction damper is used in the linear aeroelastic system.

Acknowledgements

This work was supported by an AFOSR Grant "Dynamics and Control of Nonlinear Fluid-Structure Interaction" under the direction of Dr. Dean Mook. All numerical calculations were done on a supercomputer in the North Carolina Supercomputing Center (NCSC).

References

[1] D.M. Tang, H.P. Gavin, E.H. Dowell, Study of airfoil gust response alleviation using an Electro-magnetic dry friction damper, Part 1: theory, Journal of Sound and Vibration 269 (3–5) (2003) 853–874, this issue.
[2] H.P. Gavin, J. Hoagg, M. Dobossy, Optimal design of MR dampers, Proceedings of the US–Japan Workshop on Smart Structures for Improved Seismic Performance in Urban Regions, August, Seattle WA, 2001, pp. 225–236.
[3] D.M. Tang, G.A. Cizmas, Paul, E.H. Dowell, Experiments and analysis for a gust generator in a wind tunnel, Journal of Aircraft 33 (1) (1996) 139–148.
[4] D.M. Tang, D. Kholodar, E.H. Dowell, Nonlinear response of a typical airfoil section with control surface freeplay to gust loads, American Institute of Aeronautics and Astronautics Journal 38 (9) (2000) 1543–1557.